ELSEVIER

Skalak's extended theory of water hammer

Arris S. Tijsseling[a],[*], Martin F. Lambert[b],[1], Angus R. Simpson[b],[1],
Mark L. Stephens[b],[1], John P. Vítkovský[c], Anton Bergant[d],[2]

[a]Department of Mathematics and Computer Science, Eindhoven University of Technology, Den Dolech 2, P.O. Box 513,
5600 MB Eindhoven, The Netherlands
[b]Water Systems Research Group, School of Civil and Environmental Engineering, University of Adelaide, Adelaide 5005, Australia
[c]Water Assessment Group, Department of Natural Resources and Water, Queensland Government, Indooroopilly,
QLD 4068, Australia
[d]Litostroj E.I. d.o.o., Litostrojska 50, 1000 Ljubljana, Slovenia

Abstract

Half a century ago Richard Skalak [see T.C. Skalak, A dedication in memoriam of Dr. Richard Skalak, *Annual Review of Biomedical Engineering* 1 (1999) 1–18] published a paper with the title "An extension of the theory of water hammer" [R. Skalak, An Extension of the Theory of Water Hammer, PhD Thesis, Faculty of Pure Science, Columbia University, New York, USA, 1954; R. Skalak, An extension of the theory of water hammer, *Water Power* 7/8 (1955/1956) 458–462/ 17–22; R. Skalak, An extension of the theory of water hammer, *Transactions of the ASME* 78 (1956) 105–116], which has been the basis of much subsequent work on hydraulic transients with fluid–structure interaction (FSI). The paper considers the propagation of pressure waves in liquid-filled pipes and the coupled radial/axial response of the pipe walls. In a tribute to Skalak's work, his paper is revisited and some of his less-known results are used to assess the dispersion of pressure waves in long-distance pipelines. Skalak's theory predicts that the spreading of wave fronts due to FSI is small, at most of the order of 10 pipe diameters.

© 2007 Elsevier Ltd. All rights reserved.

1. Introduction

The classical theory of water hammer [5] describes the propagation of pressure waves in fully liquid-filled pipe systems. The theory correctly predicts extreme pressures and wave periods, but it usually fails in accurately calculating damping [6] and dispersion [7] of wave fronts. In particular, field measurements usually show much more damping and dispersion than the corresponding standard water-hammer calculations. The reason is that a number of effects are not taken into account in the standard theory. These include: dissolved

*Corresponding author. Tel.: +31 40 247 2755; fax: +31 40 244 2489.

E-mail addresses: a.s.tijsseling@tue.nl (A.S. Tijsseling), mlambert@civeng.adelaide.edu.au (M.F. Lambert),
asimpson@civeng.adelaide.edu.au (A.R. Simpson), mstephen@civeng.adelaide.edu.au (M.L. Stephens),
john.vitkovsky@nrw.qld.gov.au (J.P. Vítkovský), anton.bergant@litostroj-ei.si (A. Bergant).

[1]Tel.: +61 8 8303 5135; fax: +61 8 8303 4359.

[2]Tel.: +386 1 5824 284; fax: +386 1 5824 174.

Nomenclature

a	inner radius of pipe (m)
A	twice the ratio of fluid mass to pipe-wall mass (dimensionless)
Ai	Airy function of the first kind
c	speed of sound in unconfined fluid (m/s)
c_e	elementary (water-hammer) wave speed in fluid (m/s)
c_0	elementary (thin-plate) wave speed in pipe wall (m/s)
c_1	(water-hammer) wave speed in fluid (m/s)
c_2	(precursor) wave speed in pipe wall (m/s)
Cp_n	constant (Pa/m)
Cw_n	constant (m)
d_n	constant characterising dispersion of wave front (m³/s)
d_n^*	dimensionless d_n (dimensionless)
D_n	constant (1/s²)
E	Young's modulus of elasticity of pipe-wall material (Pa)
f_n	average wake frequency (Hz)
f_n^*	dimensionless f_n (dimensionless)
f_{ring}	ring frequency (Hz)
FSI	fluid–structure interaction
h	pipe-wall thickness (m)
I	basic integral (dimensionless)
K	bulk modulus of fluid (Pa)
L	length of pipeline (m)

L_n	length of wave front (m)
L_n^*	dimensionless L_n (dimensionless)
p_n	asymptotic solution for pressure (Pa)
p_0	initial fluid pressure for $z<0$ (Pa)
R	square of wave-speed ratio c_0/c (dimensionless)
t	time (s)
t^*	dimensionless time (dimensionless)
v_0	initial axial fluid velocity for $z<0$ (m/s)
z	axial distance along pipe (m)
z_n^*	dimensionless axial distance along pipe (dimensionless)

Greek letters

α	added mass coefficient (dimensionless)
β_n	dimensionless constant characterising propagation of wave front (dimensionless)
Γ	gamma function
λ	wavelength (m)
v	Poisson's ratio (dimensionless)
ρ_0	(initial) mass density of fluid (kg/m³)
ρ_s	mass density of pipe-wall material (kg/m³)

Subscripts

$n=1$	water hammer
$n=2$	precursor

and free air in the liquid, solidified sediment deposit at the pipe walls, unsteady friction and unsteady minor losses in the transient flow, non-elastic behaviour of the pipe-wall material, and acoustic radiation to the surroundings (for buried pipes, sub-sea pipes and rock-bored tunnels). Another omitted effect is fluid–structure interaction (FSI) [8] manifesting itself in different ways: longitudinal pipe and bend motion, rubbing and non-elastic behaviour at supports, radial pipe hoop motion (breathing), wall bending and shear near steep wave fronts, and buckling and flutter of tubes conveying flow at (very) high velocity.

Bergant et al. [9,10] studied several of the aforementioned effects in a systematic way, but they did not consider the wave dispersion due to FSI. The present investigation fills this deficiency and attempts to quantify the dispersion of steep pressure wave fronts due to dynamic effects caused by radial/axial pipe motion. The focus is on the amount of spreading of the wave front and on the frequency of oscillation generated by a step pressure load. The paper is entirely based on important theoretical work of Skalak [2]. It pays tribute to his articles published half a century ago [3,4], which form a milestone in FSI research. Skalak's work is summarised and some of his main results are further explored. Dimensionless charts are presented that characterise wave dispersion in water-filled steel and plastic pipes.

2. Skalak's problem

Skalak [2–4] considered wave propagation in an infinitely long tube of inner radius a and wall thickness h, which is filled with a fluid of density ρ_0 and elasticity K. The tube wall material has density ρ_s, elasticity E and
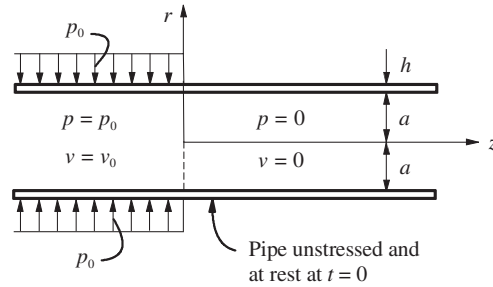
Fig. 1. Initial conditions for wave propagation (adapted from Ref. [3]).

a Poisson's ratio of v. The assumed non-equilibrium situation at time $t = 0$ is shown in Fig. 1. The pressure p and axial fluid velocity v have positive initial values p_0 and v_0 in the left half of the tube ($z < 0$), respectively, related by

$$p_0 = \rho_0 c v_0, \tag{1}$$

where

$$c = \sqrt{\frac{K}{\rho_0}}. \tag{2}$$

All other pressures, velocities and displacements are zero. These initial conditions correspond to a step wave moving in the positive axial direction ($z > 0$) at speed c. The wave would propagate in an unchanged form in a pipe with entirely rigid walls, but not so in a pipe with elastic walls.

Skalak used the following data in his test problem: $a = 0.3048$ m, $h = 4.857$ mm, $\rho_0 = 999.8$ kg/m^3, $K = 2.322$ GPa, $\rho_s = 7849$ kg/m^3, $E = 206.8$ GPa, $v = 0.3$, and herein $p_0 = 100$ kPa. Thus, $c = 1524$ m/s and $v_0 = 0.06563$ m/s.

3. Skalak's model

Skalak considered axisymmetric thin-walled tubes. His mathematical model included—in addition to standard water-hammer theory—the effects of radial inertia of liquid and pipe, and longitudinal stress waves in the pipe wall. Bending stresses and rotatory inertia in the pipe wall, that may be of importance near steep wave fronts and near pipe anchors, were also taken into account. Axisymmetric shear deformation, fluid viscosity and lobar (non-circular) modes of wall vibration were neglected. The influence of lobar modes on axial vibration is small at low frequencies because there is no significant oval–axial interaction mechanism.

3.1. FSI four-equation model

In addition, Skalak presented a simplified model that is the low-frequency limit of the two-dimensional fluid and shell representations. This so-called "FSI four-equation model" describes the axial/radial vibration of liquid-filled pipes. Two equations for the liquid are coupled with two equations for the pipe, through terms proportional to Poisson's contraction ratio, and through mutual boundary conditions. Skalak showed that the "FSI four-equation model" permits solutions that are waves of arbitrary shape travelling without dispersion at the phase velocity of either the liquid or the pipe, but he made no attempt to solve the four equations in general. The model has been validated experimentally by many researchers [8], most notably by Vardy and Fan [11], and it can be solved exactly [12,13]. This model is well-known and not pursued herein.

4. Skalak's solution

Skalak applied Fourier and Laplace transforms to find dispersion relationships for the modes of free vibration of the coupled fluid–pipe system. He applied inverse Fourier and Laplace transforms to arrive at solutions in the form of single indefinite integrals of real-valued functions. The integrals were too difficult to solve exactly, but Skalak was able to find asymptotic solutions for large values of axial distance z and time t. An important result, analysed herein, and recognised by others: "His doctoral dissertation [2] was on the water-hammer effect, and it received enough attention that the engineering director of the Grand Coulee Dam project used the theoretical results to predict pressure wave propagation effects at distances of several miles from the dam" [1].

Skalak's asymptotic solutions revealed that wave fronts spread out proportionally to the cube root of time, and that the pressure near a sharp wave front may exceed the classical Joukowsky value as a result of radial pipe/fluid vibration. Skalak predicted and quantified precursor waves in the fluid. These are pressure changes provoked by axial stress waves in the pipe wall and thus preceding the main water-hammer waves. Precursor waves were actually observed in metal and plastic pipes by Thorley [14] and by Williams [15].

The re-calculated solution to Skalak's test problem is shown to scale in Fig. 2(a). The water-hammer wave has travelled a distance of $c_1 t = 980.9$ m at time $t = 1$ s. The precursor, hardly visible at the scale of Fig. 2(a), but magnified in Fig. 2(b), has travelled a distance of $c_2 t = 5279$ m. The wave speeds c_1 and c_2 are

$$c_{1,2} = c \left\{ \frac{2AR + R + R^2(1 - v^2) \mp \sqrt{[2AR + R + R^2(1 - v^2)]^2 - 4R^2(1 - v^2)(2A + R)}}{2(2A + R)} \right\}^{1/2}, \qquad (3)$$

where c_1 has the minus sign and c_2 the plus sign, and where

$$A = \frac{\rho_0}{\rho_s} \frac{a}{h} \quad \text{and} \quad R = \left(\frac{c_0}{c} \right)^2 \qquad (4)$$

with c_0 defined below. Here $A = 7.994$ and $R = 12.47$. The water-hammer wave speed c_1 is an extension of the Korteweg formula c_e, and the precursor wave speed c_2 is approximately the wave speed in thin

(a)

(b)
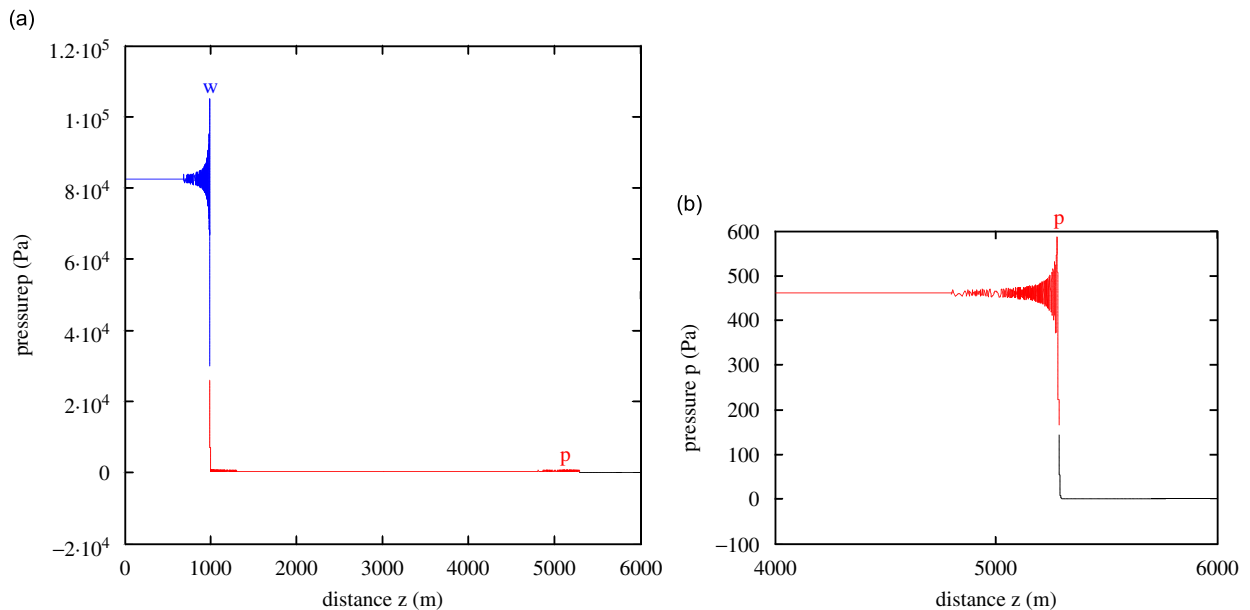
Fig. 2. Pressure as a function of distance at time $t = 1$ s: (a) water hammer with precursor wave; (b) precursor wave front (detail of (a)).

plates c_0, with

$$c_e = \frac{c}{\sqrt{1 + (2Ka/Eh)}} \quad \text{and} \quad c_0 = \sqrt{\frac{E}{\rho_s(1 - v^2)}}. \tag{5}$$

Here, $c_e = 981.9\,\text{m/s}$ and $c_0 = 5381\,\text{m/s}$.

The pressure at $z = 0$ in Fig. 2(a) is substantially lower than $p_0 = 10^5\,\text{Pa}$, because the impedance p/v (at $z = 0$) is not equal to p_0/v_0, but to $\rho_0 c_1 = (c_1/c)(p_0/v_0)$. The oscillations trailing the wave fronts are *not* due to numerical error, but predicted by the theory. Fig. 3 shows these oscillations in a non-dimensional diagram, which is assumed to be independent of the early history. The horizontal axis gives the dimensionless distance relative to the wave front,

$$z_n^* = (z - c_n t)/\sqrt[3]{d_n t}, \tag{6}$$

where the index n is 1 for the water-hammer wave and 2 for the precursor wave. The constants d_n are defined by

$$d_n = ca^2 \left\{ \frac{(A + 4)\left[(c_n/c)^5 - (c_n/c)^3(1 + R) + (c_n/c)R\right]}{-16(c_n/c)^2(2A + R) + 8R(2A + 1) + 8R^2(1 - v^2)} \right\}. \tag{7}$$

Here, $d_1 = 2.926\,\text{m}^3/\text{s}$ and $d_2 = 11.48\,\text{m}^3/\text{s}$. The original d_n given by Skalak contains a $(h/a)^2$-term that has been left out here, not only because it is small, but also because it could not be re-derived. The vertical axis in Fig. 3 gives the dimensionless wave height through the integral

$$I(\beta_n) = \frac{1}{2} - \frac{1}{\pi} \int_0^{\pm\infty} \frac{\sin(\eta + \beta_n \eta^3)}{\eta}\,\mathrm{d}\eta$$

$$= \frac{1}{3} - \int_0^{1/\sqrt[3]{3\beta_n}} \mathrm{Ai}(\xi)\,\mathrm{d}\xi, \tag{8}$$

which has been drawn as a function of $z_n^* = 1/\sqrt[3]{\beta_n}$ with

$$\beta_n = \frac{d_n t}{(z - c_n t)^3}. \tag{9}$$

The upper bound in the first integral is $+\infty$ for $\beta_n > 0$ and $-\infty$ for $\beta_n < 0$. Three integrals can be calculated analytically:

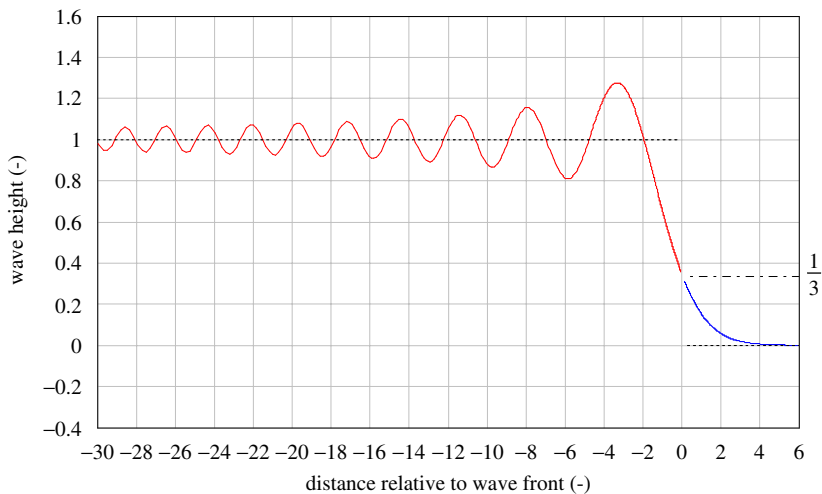$$I(0^-) = 1, \ I(0^+) = 0 \ \text{and} \ I(\pm\infty) = \tfrac{1}{3}. \tag{10}$$

Fig. 3. Wave front dispersion; horizontal axis: z_n^* (Eq. (6)) and vertical axis: I (Eq. (8)).

The other integrals have been calculated numerically for 1000 values of $|\beta_n|$ in the range 10^{-7}–10^3, with the upper bound in the first integral in Eq. (8) as large as possible [16]. Using tables of Ai—the Airy function of the first kind—Skalak [17] computed numerically the second integral in Eq. (8). The integral I, and hence the wave height, is constant when β_n is constant, which is along the curves

$$z = c_n t + \sqrt[3]{\frac{d_n t}{\beta_n}} \qquad (11)$$

in the distance–time plane. The wave front, where $\beta_n = \pm\infty$ and $1/\sqrt[3]{\beta_n} = 0$, is clearly identified as the only point travelling at both constant speed, c_n, and constant dimensionless height, $\frac{1}{3}$.

The dimensional pressure for water-hammer ($n = 1$) and precursor ($n = 2$) waves travelling in the positive z direction is (up to a constant, vertical shift):

$$p_n(\beta_n) = Cp_n Cw_n \int_0^{\pm\infty} \frac{\sin(\eta + \beta_n \eta^3)}{\eta}\, d\eta \qquad (12)$$

with

$$Cp_n = 2\rho_0 c_n^2 / a[(c_n^2/c^2) - 1], \quad Cw_n = p_0/\pi\rho_s h(c_n/c - 1)D_n,$$

$$D_n = 4\rho_0 c_n^4/\rho_s h c^2 a(c_n^2/c^2 - 1)^2 + 2c_0^2[v^2/(1 - c_0^2/c_n^2)^2 + 1 - v^2]/a^2,$$

where a $(h/a)^2$-term has been neglected in D_n. Here, $Cp_1 Cw_1 = -26{,}105\,\text{Pa}$ and $Cp_2 Cw_2 = -146.5\,\text{Pa}$.

4.1. FSI wave front spreading

From Fig. 3 it is seen that the initial step wave front spreads out, that is, the steepness of the front slope continuously diminishes. Skalak defined a measure for the length L_n of the wave front, namely the reciprocal of the slope at the point ($z_n^* = 0$, $I = \frac{1}{3}$) for the unit jump in Fig. 3. He derived the following formula:

$$L_n(t) = \frac{3\pi\sqrt[3]{d_n t}}{\Gamma(\frac{1}{3})\sin(\frac{\pi}{3})} \approx 4\sqrt[3]{d_n t}, \qquad (13)$$

where Γ is the gamma function. For the data given in Skalak's test problem, $L_1(1\,\text{s}) = 5.810\,\text{m}$ (water-hammer wave) and $L_2(1\,\text{s}) = 9.163\,\text{m}$ (precursor wave), as shown in Fig. 4. The length of the wave front increases proportionally to the cube root of time t. For non-step excitation one might start at the proper initial length in Fig. 4, noting that the diagram is *not* valid for small t, say $t < 1\,\text{s}$.

4.2. FSI wave front oscillation

From Fig. 3 it is seen that the passage of a wave front causes a decaying oscillation of increasing frequency. The maximum overshoot is 1.2744, where the classical Joukowsky value would be 1. The average frequency
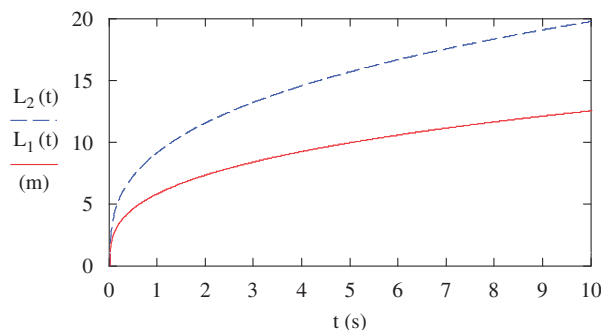

Fig. 4. Wave front spreading. Lengths of water hammer (L_1, solid line) and precursor (L_2, dashed line) wave fronts as a function of time.
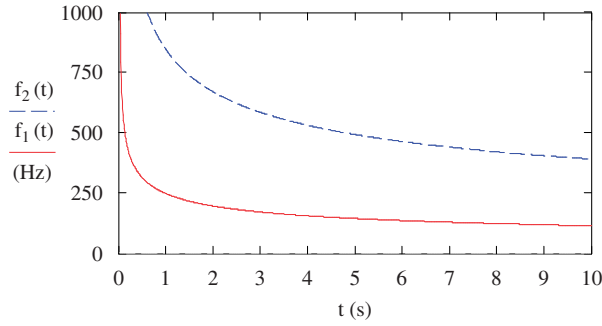
Fig. 5. Wave front oscillation. Average frequencies of water hammer (f_1, solid line) and precursor (f_2, dashed line) waves as a function of time.

estimated from the 10 maxima in Fig. 3, propagating at almost the speed c_n, is

$$f_n(t) \approx 0.36 \frac{c_n}{\sqrt[3]{d_n t}} \approx 1.44 \frac{c_n}{L_n}. \tag{14}$$

This average frequency decreases in time as displayed in Fig. 5. The average frequency f_1 decreases from about 250 Hz at $t = 1$ s to about 100 Hz at $t = 10$ s, which is much lower than the ring frequency of a freely vibrating pipe hoop,

$$f_{\text{ring}}(\alpha) = \frac{1}{2\pi a} \sqrt{\frac{E}{\rho_s + \alpha(a/h)\rho_0}}, \tag{15}$$

where the coefficient α determines the added fluid mass. In the literature values of α of $\frac{1}{4}$, $\frac{1}{3}$ and $\frac{1}{2}$ have been proposed [18–21], depending on the assumed distribution of the radial fluid velocity. Here, the values $f_{\text{ring}}(\frac{1}{4}) = 1550$ Hz, $f_{\text{ring}}(\frac{1}{3}) = 1400$ Hz and $f_{\text{ring}}(\frac{1}{2}) = 1200$ Hz are much higher than the values of f_1 ($t > 1$ s) in Fig. 5. Interaction with longitudinal fluid and pipe modes has been totally ignored in the derivation of f_{ring}. The cut-on frequency of the lowest lobar mode (ovaling) of vibration is 16 Hz [16].

5. Dimensionless charts

Introducing the dimensionless quantities

$$t^* = \frac{c}{a}t, \quad L_n^* = \frac{L_n}{a}, \quad f_n^* = \frac{a}{c}f_n, \quad c_n^* = \frac{c_n}{c}, \quad d_n^* = \frac{d_n}{ca^2}, \tag{16}$$

Eqs. (13) and (14) become

$$L_n^*(t^*) \approx 4\sqrt[3]{d_n^* t^*} \tag{17}$$

and

$$f_n^*(t^*) \approx 0.36 \frac{c_n^*}{\sqrt[3]{d_n^* t^*}}. \tag{18}$$

The parameters c_n^* and d_n^* depend on A, R and v. The wave speed c in Eq. (16) depends only on the properties of the contained fluid, and c is about 1500 m/s for water. It should be noted that for water-hammer problems the real time t is related to t^* by $t = (a/c)t^* = (c_1/c)(a/L)(L/c_1)t^*$, where L is the length of the pipeline and L/c_1 is the fundamental time scale in water hammer.
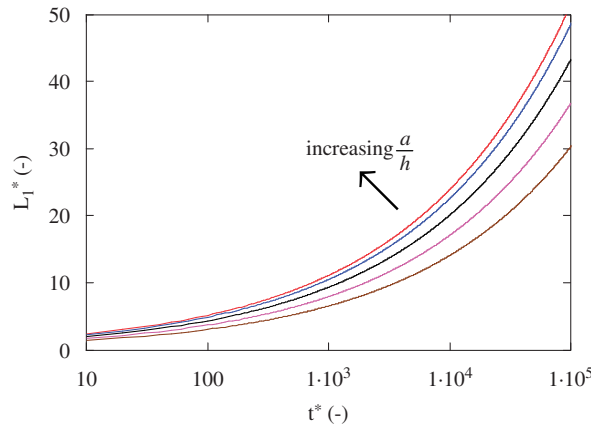
Fig. 6. Water-filled steel pipe. Water-hammer wave front length $L_1^* = L_1/a$ as a function of time $t^* = ct/a$ for five different values of a/h. From top line to bottom line: $a/h = 80, 40, 20, 10$ and 5.
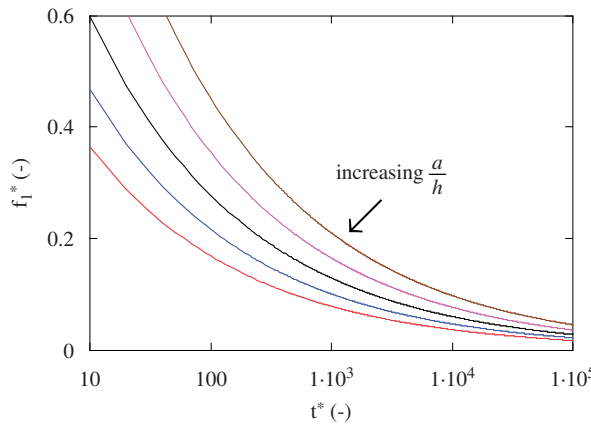

Fig. 7. Water-filled steel pipe. Water-hammer wave front frequency $f_1^* = af_1/c$ as a function of time $t^* = ct/a$ for five different values of a/h. From top line to bottom line: $a/h = 5, 10, 20, 40$ and 80.

5.1. Water-filled steel pipe

Typical values of A, R and v for a water-filled *steel* pipe are: $A = (1/8)(a/h)$, $R = 12.5$ and $v = 0.3$. Fig. 6 displays the dependence of $L_1^*(t^*)$ on the ratio a/h of pipe radius to wall thickness. The length of the water-hammer wave front is at most of the order of 10 pipe diameters, and thicker pipe walls lead to shorter wave fronts. Correspondingly, thicker pipe walls give higher frequencies of wave front oscillation, as shown in Fig. 7.

5.2. Water-filled plastic pipe

In plastic pipes viscoelastic behaviour of the wall material influences wave dynamics [9,22], but in the vicinity of steep wave fronts an instantaneous elastic response is expected instead of a retarded viscous response. Additionally, the strong dependence of c_1 on a/h in plastic pipes makes it worthwhile pursuing the elastic approximation.

Typical values of A, R and v for a water-filled *plastic* pipe are: $A = a/h$, $R = 1$ and $v = 0.4$. Because $R = 1$, the dimensionless wave speeds are $c_1^* = \sqrt{(1 - v^2)/(2A + 1)}$ and $c_2^* = 1$, so that the precursor wave speed c_2
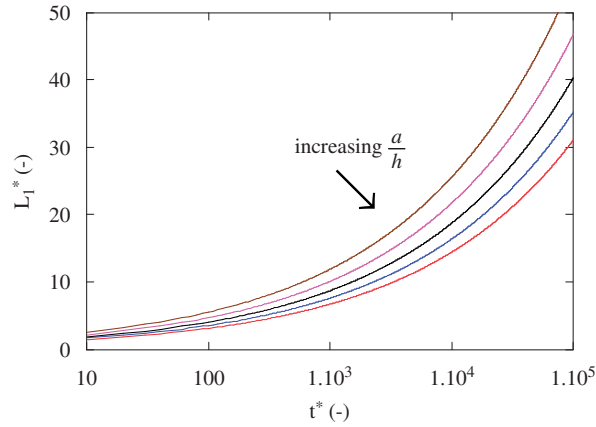
Fig. 8. Water-filled plastic pipe. Water-hammer wave front length $L_1^* = L_1/a$ as a function of time $t^* = ct/a$ for five different values of a/h. From top line to bottom line: $a/h = 5$, 10, 20, 40 and 80.
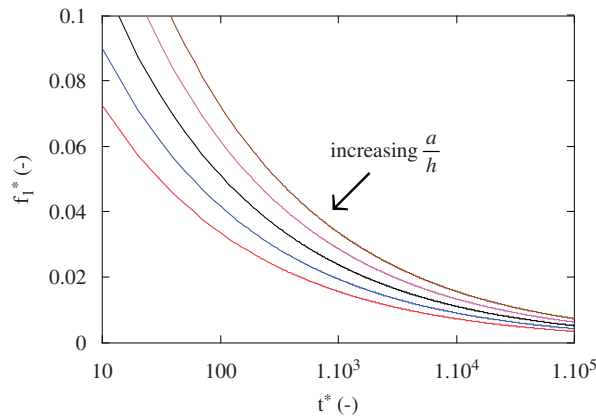

Fig. 9. Water-filled plastic pipe. Water-hammer wave front frequency $f_1^* = af_1/c$ as a function of time $t^* = ct/a$ for five different values of a/h. From top line to bottom line: $a/h = 50$, 10, 20, 40 and 80.
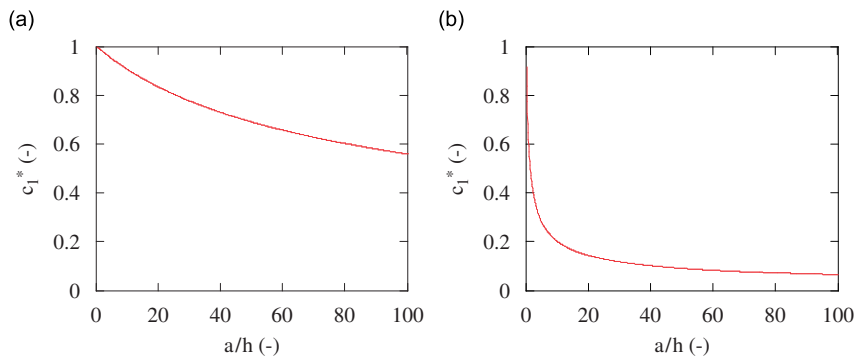

Fig. 10. Water-hammer wave speed $c_1^* = c_1/c$ as a function of a/h, for (a) water-filled steel pipe and (b) water-filled plastic pipe.

is independent of A and v. Figs. 8 and 9 display $L_1^*(t^*)$ and $f_1^*(t^*)$. Like the steel pipe, the wave front length is of the order of 10 diameters, but—surprisingly—the front length decreases for increasing ratio a/h. This means that for given pipe radius, thicker pipe walls cause more dispersion. Further investigation of this fact showed

that for a very thin-walled *steel* pipe the same phenomenon occurs: for ratios a/h larger than 112, L_1^* decreases for increasing a/h. Similarly, for very thick-walled *plastic* pipes, with a/h smaller than 0.24, L_1^* decreases for decreasing a/h. This behaviour can be explained from the strong a/h-dependence of the wave-speed ratio $c_1/c = c_1^*$, shown in Fig. 10, as a consequence of pipe hoop elasticity. The plastic pipe (Fig. 10(b)) has much smaller values of c_1/c than the corresponding steel pipe (Fig. 10(a)), and this has according to Eq. (7) a strong effect on d_n^*. The much smaller values of $c_1^* = c_1/c$ also explain (see Eq. (18)) that the frequencies in the plastic pipe (see Fig. 9) are much smaller than the corresponding frequencies in the steel pipe (see Fig. 7).

6. Practical considerations

Skalak's theory describes reflection-free wave propagation in long liquid-filled pipes. In cross-country pipelines, the pressure waves in the liquid may travel long distances without significant reflection, but the stress waves in the wall will meet pipe supports and/or anchors at regular intervals. The stress waves will partly reflect from these supports, and most likely non-axisymmetric bending will be generated. The influence of these reflections on Skalak's results is unknown.

Skalak's instantaneous and flat excitation is difficult to realise in practice [23]. Only the collapse of column separations [24] and the impact of gas shock waves [25–28] may be similar to such an extreme excitation. This means that the trailing oscillations associated with radial vibration will be difficult to generate.

The smoothing of the wave front is found to be very small and will be difficult to distinguish from other damping effects in laboratory tests and field measurements. For example, in an analysis similar to Skalak's, Bahrar et al. [29] have shown that fluid viscosity has a significant long-term effect on the dispersion of the wave front.

Skalak's asymptotic solution is valid for large time t and z (compared to radius a). In his approximations, terms of the order of $1/\sqrt{t}$ have been neglected, which formally means that $t \gg 1$. Unfortunately, Skalak has not made the time t non-dimensional. Also, long wavelength approximations have been made, where the wavelength $\lambda \gg 2\pi a$ and $\lambda > 2\pi\sqrt{d_1/c_1}$, although the local behaviour near wave fronts includes short wavelengths. The loss of accuracy caused by the truncation of several integrals is another matter of concern. Nevertheless, Skalak's dispersion theory has been partly confirmed by others in the impact of elastic bars [17,23,30] and in water hammer in liquid-filled pipes [29,31,32].

7. Conclusion

Skalak's asymptotic solution describing the propagation and dispersion of water hammer ($n = 1$) and precursor ($n = 2$) waves has been investigated. The solution is shown in the "universal" Fig. 3 and it is valid for large $z_n = c_n t$. Skalak defined the important length scale $\sqrt[3]{d_n t}$, which stretches the wave front and trailing oscillation in Fig. 3. Skalak presented results for one test problem, the solution of which is shown to scale in Fig. 2. New estimates of front length and average frequency of oscillation are given for a range of situations in dimensionless diagrams (Figs. 6–9). The main conclusion from these diagrams is that in unrestrained water-filled steel and plastic pipes wave front spreading due to FSI is small, at most of the order of 10 pipe diameters.

Acknowledgement

References

[1] T.C. Skalak, A dedication in memoriam of Dr. Richard Skalak, *Annual Review of Biomedical Engineering* 1 (1999) 1–18.
[2] R. Skalak, An Extension of the Theory of Water Hammer, PhD Thesis, Faculty of Pure Science, Columbia University, New York, USA, 1954.

[3] R. Skalak, An extension of the theory of water hammer, *Water Power* 7/8 (1955/1956) 458–462/17–22.

[4] R. Skalak, An extension of the theory of water hammer, *Transactions of the ASME* 78 (1956) 105–116.

[5] E.B. Wylie, V.L. Streeter, *Fluid Transients in Systems*, Prentice-Hall, Englewood Cliffs, NJ, USA, 1993.

[6] D.J. Leslie, A.S. Tijsseling, Travelling discontinuities in water hammer theory: attenuation due to friction, in: A. Anderson (Ed.), *Proceedings of the Eighth International Conference on Pressure Surges*, Published by BHR Group, Cranfield, UK, and Professional Engineering Publishing, Bury St Edmunds, UK, 2000, pp. 323–335.

[7] A.E. Vardy, J.M.B. Brown, Friction-dependent wavefront evolution, in: A. Anderson (Ed.), *Proceedings of the Eighth International Conference on Pressure Surges*, Published by BHR Group, Cranfield, UK, and Professional Engineering Publishing, Bury St. Edmunds, UK, 2000, pp. 337–349.

[8] D.C. Wiggert, A.S. Tijsseling, Fluid transients and fluid–structure interaction in flexible liquid-filled piping, *ASME Applied Mechanics Reviews* 54 (2001) 455–481.

[9] A. Bergant, A.S. Tijsseling, J.P. Vítkovský, D. Covas, A.R. Simpson, M.F. Lambert, Parameters affecting water-hammer wave attenuation, shape and timing—part 1: mathematical tools, *IAHR Journal of Hydraulic Research* 46 (2008), in press.

[10] A. Bergant, A.S. Tijsseling, J.P. Vítkovský, D. Covas, A.R. Simpson, M.F. Lambert, Parameters affecting water-hammer wave attenuation, shape and timing—part 2: case studies, *IAHR Journal of Hydraulic Research* 46 (2008), in press.

[11] A.E. Vardy, D. Fan, Flexural waves in a closed tube, in: A.R.D. Thorley (Ed.), *Proceedings of the Sixth International Conference on Pressure Surges*, BHRA, Cambridge, UK, 1989, pp. 43–57.

[12] A.S. Tijsseling, Exact solution of linear hyperbolic four-equation system*s* in axial liquid-pipe vibration, *Journal of Fluids and Structures* 18 (2003) 179–196.

[13] Q.S. Li, K. Yang, L. Zhang, Analytical solution for fluid-structure interaction in liquid-filled pipes subjected to impact-induced water hammer, *ASCE Journal of Engineering Mechanics* 129 (2003) 1408–1417.

[14] A.R.D. Thorley, Pressure transients in hydraulic pipelines, *ASME Journal of Basic Engineering* 91 (1969) 453–461.

[15] D.J. Williams, Water-hammer in non-rigid pipes: precursor waves and mechanical damping, *IMechE Journal of Mechanical Engineering Science* 19 (1977) 237–242.

[16] A.S. Tijsseling, M.F. Lambert, A.R. Simpson, M.L. Stephens, J.P. Vítkovský, A. Bergant, Wave front dispersion due to fluid–structure interaction in long liquid-filled pipelines, CASA Report 06-27, ISSN 0926-4507, Department of Mathematics and Computer Science, Eindhoven University of Technology, Eindhoven, The Netherlands, 2006.

[17] R. Skalak, Longitudinal impact of a semi-infinite circular elastic bar, *ASME Journal of Applied Mechanics* 24 (1957) 59–64.

[18] F. Barez, W. Goldsmith, J.L. Sackman, Longitudinal waves in liquid-filled tubes—II. Experiments, *International Journal of Mechanical Sciences* 21 (1979) 223–236.

[19] A. Kellner, C. Schönfelder, The effect of fluid/structure interaction on pressure pulse loads on pipes, *3R International* 21 (1982) 443–449 (in German).

[20] J.S. Walker, J.W. Phillips, Pulse propagation in fluid-filled tubes, *ASME Journal of Applied Mechanics* 44 (1977) 31–35.

[21] A.S. Tijsseling, Fluid–Structure Interaction in Case of Water Hammer with Cavitation, PhD Thesis, Faculty of Civil Engineering, Delft University of Technology, Communications on Hydraulic and Geotechnical Engineering, Report No. 93-6, ISSN 0169-6548, Delft, The Netherlands, 1993. Available from ⟨http://www.darenet.nl/en/page/language.view/search.page⟩.

[22] D. Covas, I. Stoianov, J.F. Mano, H. Ramos, N. Graham, C. Maksimovic, The dynamic effect of pipe-wall viscoelasticity in hydraulic transients, part II—model development, calibration and verification, *IAHR Journal of Hydraulic Research* 43 (2005) 56–70.

[23] E.C.H. Becker, H.D. Conway, Generation and use of mechanical step transients in dynamic measurement, *British Journal of Applied Physics* 15 (1964) 1225–1231.

[24] A. Bergant, A.R. Simpson, A.S. Tijsseling, Water hammer with column separation: a historical review, *Journal of Fluids and Structures* 22 (2006) 135–171.

[25] G.A.A. Asselman, Een onderzoek naar de schokvorm in de enkel-bel schokbuis, alsmede een literatuurstudie van het gedrag van gasbellen in water, MSc Thesis, Report R-77-A, Department of Applied Physics, Eindhoven University of Technology, Eindhoven, The Netherlands, 1969 (in Dutch).

[26] C.J. Wisse, On Frequency Dependence of Acoustic Waves in Porous Cylinders, PhD Thesis, Faculty of Geosciences, Delft University of Technology, Delft, The Netherlands, 1999. Available from ⟨http://www.darenet.nl/en/page/language.view/search.page⟩.

[27] G.E. Chao, Dispersive Surface Acoustic Waves in Poroelastic Media, PhD Thesis, Faculty of Geosciences, Delft University of Technology, Delft, The Netherlands, 2005. Available from ⟨http://www.darenet.nl/en/page/language.view/search.page⟩.

[28] Sh. Suzuki, Dynamic behaviour of thin cylindrical shells subjected to high-speed travelling inner pressures, *Ingenieur-Archiv* 42 (1972) 69–79.

[29] B. Bahrar, E. Rieutord, R. Morel, G. Zeggwagh, Modeling of the water-hammer phenomenon with respect to real pipe behavior, *La Houille Blanche – Revue Internationale de l'Eau* 53 (1998) 18–25 (in French).

[30] F. Valeš, Š. Morávka, R. Brepta, J. Červ, Wave propagation in a thick cylindrical bar due to longitudinal impact, *JSME International Journal, Series A* 39 (1996) 60–70.

[31] T. Adachi, S. Ujihashi, H. Matsumoto, Impulsive responses of a circular cylindrical shell subjected to water hammer waves, *ASME Journal of Pressure Vessel Technology* 113 (1991) 517–523.

[32] D. Sumarsono, Onde de pression dans un liquide confiné par un tube souple, PhD Thesis, Department of Mechanical Engineering, University of Orleans, Orleans, France, 1993 (in French).